UCLA
COMPUTATIONAL AND APPLIED MATHEMATICS

Convergence of the Alternating Minimization Algorithm for Blind Deconvolution

Tony F. Chan
C.K. Wong

June 1999

CAM Report 99-19

Department of Mathematics
University of California, Los Angeles
Los Angeles, CA. 90095-1555

http://www.math.ucla.edu/applied/cam/index.html

CONVERGENCE OF THE ALTERNATING MINIMIZATION ALGORITHM FOR BLIND DECONVOLUTION

TONY F. CHAN * AND C.K. WONG †

Abstract. Blind deconvolution refers to the image processing task of restoring the original image from a blurred version, without knowledge of the blurring function. One approach that has been proposed recently [3, 11] is a joint minimization model in which an objective function is set up consisting of three terms: the data fitting term, and the regularization terms for the image and the blur. This model implicitly defines a one-parameter family of blurred images and PSFs, from which the user can decide, usually using additional information, which is the "best" restored image. To find a local minimum of the objective function, we use an alternating minimization procedure [11] in which we fix either the blur or the image and minimize respect to the other variable, each step of which is a standard non-blind deconvolution problem. While the model is not convex and thus allows multiple solutions, we have found that the alternating minimization procedure always converges globally, but with the converged solution depending on the initial guess. In this paper, we will give an analysis of the alternating minimization procedure which will explain the convergence behavior and the observed robustness of the method.

1. Introduction and summary. Image restoration refers to recovering the original scene from observations polluted by blurring and noise. If u^{true} and z denote the original and observed images respectively, the linear shift-invariant image degradation model can be expressed as:

$$(1) \quad z(x,y) = \int_\Omega h^{true}(x-s, y-t) u_{true}(s,t)\, ds\, dt + \eta(x,y) \equiv h_{true} \star u_{true} + \eta.$$

Here the domain Ω is a rectangle $[-L_x, L_x] \times [-L_y, L_y]$, $\star$ denotes the convolution operator, h^{true} is a point spread function (PSF) (i.e, $h^{true} \geq 0$ and $\int_\Omega h^{true} = 1$) and η is a white Gaussian noise with zero mean. The blind image deconvolution problem refers to restoring both the image u and the blurring function h while given only the observed image z and probably some statistics of the noise η. There are many existing algorithms for simultaneously identify u and h, see for instance, [5, 4, 7, 10, 11].

As the blind deconvolution problem is ill-posed with respect to both the image and the blurring function, a joint regularization technique [3, 11] was recently developed to regularize both u and h. More specifically, these papers considered the joint minimization problem:

$$(2) \qquad \min_{u,h} f(u,h) \equiv \min_{u,h} \|h \star u - z\|_{L^2}^2 + \alpha_1 r(u) + \alpha_2 r(h).$$

Here α_1 and α_2 are positive parameters which measure the trade off between a good fit and the regularity of the solutions u and h. Typical choices of regularization functionals $r(u)$ and $r(h)$ that can be found in the literature are the H^1 regularization

* Tony Chan is with the Department of Mathematics, University of California, Los Angeles, 405 Hilgard Avenue, Los Angeles, CA 90095-1555. Email: chan@math.ucla.edu, WWW: http://www.math.ucla.edu/~ chan.

† C.K. Wong is with the Department of Mathematics, University of California, Los Angeles, 405 Hilgard Avenue, Los Angeles, CA 90095-1555. Email: ckwong@math.ucla.edu.

Both authors are supported by the ONR under Contract N00014-96-1-0277, and by the NSF under Grant DMS 96-26755. C.K. Wong is also supported by the Sloan dissertation year fellowship.

AM Algorithm – min h then min u (AMHU) :

Given u^0: iterating $k = 1, 2, \ldots$

- solve $h^k = \arg\min_h f(u^{k-1}, h)$ by solving the corresponding Euler-Lagrange equation:

$$0 = \nabla_h f(u^{k-1}, h) \equiv 2u^{k-1}(-x,-y) \star (u^{k-1}(x,y) \star h(x,y) - z) + \alpha_2 R(h)$$

$$\frac{\partial h}{\partial n} = 0 \quad \text{on} \quad \partial\Omega$$

- solve $u^k = \arg\min_u f(u, h^k)$ by solving the corresponding Euler-Lagrange equation:

$$0 = \nabla_u f(u, h^k) \equiv 2h^k(-x,-y) \star (h^k(x,y) \star u(x,y) - z) + \alpha_1 R(u)$$

$$\frac{\partial u}{\partial n} = 0 \quad \text{on} \quad \partial\Omega$$

AM Algorithm – min u then min h (AMUH) :

Given h^0: iterating $k = 1, 2, \ldots$

- solve $u^{k-1} = \arg\min_u f(u, h^{k-1})$ by solving the corresponding Euler-Lagrange equation:

$$0 = \nabla_u f(u, h^{k-1}) \equiv 2h^{k-1}(-x,-y) \star (h^{k-1}(x,y) \star u(x,y) - z) + \alpha_1 R(u)$$

$$\frac{\partial u}{\partial n} = 0 \quad \text{on} \quad \partial\Omega$$

- solve $h^k = \arg\min_h f(u^{k-1}, h)$ by solving the corresponding Euler-Lagrange equation:

$$0 = \nabla_h f(u^{k-1}, h) \equiv 2u^{k-1}(-x,-y) \star (u^{k-1}(x,y) \star h(x,y) - z) + \alpha_2 R(h)$$

$$\frac{\partial h}{\partial n} = 0 \quad \text{on} \quad \partial\Omega$$

TABLE 1

AMHU (top): Minimize h first then u. AMUH (bottom): Minimize u first then h.

[11] and the *Total variation* (TV) regularization [9, 8, 12]:

$$H^1(u) \equiv \int_\Omega |\nabla u|^2 \, dx \, dy, \qquad TV(u) \equiv \int_\Omega |\nabla u| \, dx \, dy,$$

which are designed to penalize oscillations in u and h as they are reflected in large derivatives. We remark that the TV–norm allows discontinuities in both u and h, thus making it superior to the H^1 regularization in cases where either h or u can have discontinuities (e.g. edges in u and out-of-focus blur). We also remark that the parameter α_1 can be determined from the signal to noise ratio (SNR), see [1, 9]. Hence, the model (2) defines a one-parameter (α_2) family of deconvoluted images u and PSFs h, from which the user can decide, usually using additional information, which is the "best" restored image.

Note that $f(u, h)$ as a two variables functional is not convex and hence allows infinitely many solutions. In fact, if (u, h) is a solution, then so are $(-u, -h)$, $(\frac{\alpha_2}{\alpha_1}h, \frac{\alpha_1}{\alpha_2}u)$, $(u(x \pm c, y \pm d), h(x \mp c, y \mp d))$ for any real constant c and d. To find a local minimizer, You and Kaveh [11] observed that for a fixed h (resp u), $f(\cdot, h)$ is a convex function of u (resp h) and they proposed the alternating minimization (AM) algo-

rithm; see Table 1. With an initial guess u^0 for u, we can minimize (2) by first solving $f(u^0, h^1) \equiv \min_h f(u^0, \cdot)$, and then $f(u^1, h^1) \equiv \min_u f(\cdot, h^1)$. These convex minimization problems can be solved by solving respectively the corresponding Euler-Lagrange equations,

$$0 = \nabla_h f(u^0, h) \equiv 2u^0(-x, -y) \star (u^0(x, y) \star h(x, y) - z) + \alpha_2 R(h)$$

$$\frac{\partial h}{\partial n} = 0 \quad \text{on} \quad \partial\Omega \tag{3}$$

and

$$0 = \nabla_u f(u, h^1) \equiv 2h^1(-x, -y) \star (h^1(x, y) \star u(x, y) - z) + \alpha_1 R(u)$$

$$\frac{\partial u}{\partial n} = 0 \quad \text{on} \quad \partial\Omega, \tag{4}$$

where

$$R(u) = -2\Delta u \qquad \text{and} \qquad R(h) = -2\Delta h, \tag{5}$$

if $r(\cdot)$ is the H^1 regularization (see [11]) or

$$R(u) = -\nabla \cdot \left(\frac{\nabla u}{|\nabla u|}\right) \qquad \text{and} \qquad R(h) = -\nabla \cdot \left(\frac{\nabla h}{|\nabla h|}\right) \tag{6}$$

if $r(\cdot)$ is the TV regularization (see [3]). Here Δ denotes the 2D Laplacian operator. The formulas (5) and (6) are obtained by taking the gradient of $H^1(\cdot)$ and $TV(\cdot)$ and then applying integration by parts from which the Neumann boundary conditions in (3) and (4) arise. We called this approach, by first minimizing h and then u, the AMHU algorithm. A variant of the AM algorithm is to minimize with respect to u first and then h, which we call the AMUH algorithm; see bottom part of Table 1. Now in each AM iteration, we are solving two convex non-blind deconvolution problems, one for h^k with known u^{k-1} and one for u^k with known h^k, in which the corresponding Euler-Lagrange equations are being solved. By alternately minimizing f, the function value $f(u^k, h^k)$ decreases as k increases. We remark that the initial guesses h^0 and u^0 are usually chosen to be the delta function $\delta(x, y)$ and the observed image z respectively, as often these are the only available information in practice.

It has been demonstrated numerically in [3, 11] that the AM algorithm converges very fast and produces a very good restored image after only a few AM iterations. However, the minimization problem in (2) is non-convex and has more than one minimizer. Therefore, analyzing the convergence behavior of the AM iteration is crucial for understanding which local minimizer the AM algorithm converges to and how this minimizer depends on the initial guesses for u and h. In practice, images are often represented as two dimensional grid functions defined on discrete spaces (for example, $\{(i, j) | \, i = 0, 1, \ldots, m-1, \; j = 0, 1, \ldots, n-1\}$). In §2, we will discretize the functional in (2) and consider the discrete version of the AM algorithm. We will prove in §3 that the discrete version of the AM algorithm converges to a local minimizer for any given initial guess and we will discuss how the limit depends on the initial guess. The analysis will be for the case of H^1 regularization only as the TV regularization is highly nonlinear and thus is not as easily analyzed.

To simplify the analysis, we will also change the Neumann boundary conditions in (3) and (4) to periodic ones, a practice commonly employed to allow a Fourier analysis to be used. Numerical results indicates that the analysis for the periodic case provides a very good prediction for the Neumann boundary condition. We will prove that the AMHU and AMUH algorithms are equivalent in the sense that AMHU algorithm with initial guess u^0 can produce the same iterates as AMUH if h^0 is properly initialized and vice versa. Notice that if *a priori* information about the image or the PSF is available, for example that $\int_\Omega h^{true}(p,q) = 1$, or h_{true} is even or $u^{true}(p,q) \geq 0$, we may introduce such additional constraints in (2) or simply project the iterate from each AM iteration by $h^k \leftarrow h^k / \int_\Omega h^k$, $h^k(x,y) \leftarrow 0$ if $h^k(x,y) < 0$, $h^k(x,y) \leftarrow (h^k(x,y) + h^k(-x,-y))/2$ and $u^k(x,y) \leftarrow 0$ if $u^k(x,y) < 0$ respectively. Our analysis shows that these properties are automatically preserved by the AM algorithm and thus it is unnecessary to impose them explicitly. Finally, we will discuss some of the possible limitations of the H^1 regularization. Numerical results supporting our theoretical result will be given in §4.

2. Discretization and Boundary Conditions. In this section, we consider both the discrete version of the minimization problem (2) and the discrete version of the AM algorithm. Suppose we discretize the domain Ω with m pixels in the x-direction and n pixels in the y-direction. Let us denote the original m–by–n discrete image as a vector by

$$u^{true} = [u(p,q)]_{p=0,\ldots,m-1,q=0,\ldots,n-1}$$

and the PSF by

$$h^{true} = [h^{true}(p,q)]_{p=0,\ldots,m-1,q=0,\ldots,n-1}$$

where lexicographical ordering is used. Then we can express (1) as

$$z = H^{true}u^{true} + \eta,$$

where H^{true} corresponds to the blurring matrix associated with h^{true}. With these notations, the minimization problem (2) has the following discrete form:

$$\begin{aligned} \min_{u,h} f(u,h) &\equiv \min_{u,h} \tfrac{1}{2}\|h \star u - z\|^2 + \alpha_1 r(u) + \alpha_2 r(h) \\ &= \min_{u,h} \|Hu - z\|_2^2 + \alpha_1 r(u) + \alpha_2 r(h), \end{aligned} \tag{7}$$

where H corresponds to the blurring matrix associated with the unknown blur h. The discrete TV norm and the discrete H^1 norm are expressed as

$$H^1(u) \equiv \sum_{p=0}^{m-1}\sum_{q=0}^{n-1} |\nabla u(p,q)|^2, \qquad TV(u) \equiv \sum_{p=0}^{m-1}\sum_{q=0}^{n-1} |\nabla u(p,q)|. \tag{8}$$

Here $|\nabla u(p,q)|^2 = (u(p+1,q) - u(p,q))^2 + (u(p,q+1) - u(p,q))^2$ is the square of the norm of a discrete gradient at (p,q). Now, the discrete AM algorithm is expressed in Table 2.

To simplify the analysis on the AM algorithm, we will change the Neumann boundary conditions in (3) and (4) to periodic ones. That is, we assume that

$$u(p+m, q+n) = u(p,q) \qquad \text{and} \qquad h(p+m, q+n) = h(p,q)$$

Discrete AM Algorithm – min h then min u (AMHU) :
Given u^0: iterating $k = 1, 2, \ldots$

- solve $h^k = \arg\min_h f(u^{k-1}, h)$ by solving the corresponding Euler-Lagrange equation:
  $0 = \nabla_h f(u^{k-1}, h) \equiv 2U^{k-1*}(U^{k-1}h - z) - \alpha_2 \nabla_h r(h)$
- solve $u^k = \arg\min_u f(u, h^k)$ by solving the corresponding Euler-Lagrange equation:
  $0 = \nabla_u f(u, h^k) \equiv 2H^{k*}(H^k u - z) - \alpha_1 \nabla_u r(u)$

Discrete AM Algorithm – min u then min h (AMUH) :
Given h^0: iterating $k = 1, 2, \ldots$

- solve $u^{k-1} = \arg\min_u f(u, h^{k-1})$ by solving the corresponding Euler-Lagrange equation:
  $0 = \nabla_u f(u, h^{k-1}) \equiv 2H^{k-1*}(H^{k-1}u - z) - \alpha_1 \nabla_u r(u)$
- solve $h^k = \arg\min_h f(u^{k-1}, h)$ by solving the corresponding Euler-Lagrange equation:
  $0 = \nabla_h f(u^{k-1}, h) \equiv 2U^{k-1*}(U^{k-1}h - z) - \alpha_2 \nabla_h r(h)$

TABLE 2
Discrete AMHU (top): Minimize h first then u. Discrete AMUH (bottom): Minimize u first then h.

for any integers p and q. Now the blurring matrix H is a block circulant matrix with circulant blocks of the form:

$$H = \begin{pmatrix} H_0 & H_{m-1} & \cdots & H_2 & H_1 \\ H_1 & H_0 & H_{m-1} & & H_2 \\ \vdots & H_1 & H_0 & \ddots & \vdots \\ H_{m-2} & & \ddots & \ddots & H_{m-1} \\ H_{m-1} & H_{m-2} & \cdots & H_1 & H_0 \end{pmatrix}, \tag{9}$$

where each sub-block H_p is a circulant matrix defined as

$$H_p = \begin{pmatrix} h(p,0) & h(p,n-1) & \cdots & h(p,2) & h(p,1) \\ h(p,1) & h(p,0) & h(p,n-1) & & h(p,2) \\ \vdots & h(p,1) & h(p,0) & \ddots & \vdots \\ h(p,n-2) & & \ddots & \ddots & h(p,n-1) \\ h(p,n-1) & h(p,n-2) & \cdots & h(p,1) & h(p,0) \end{pmatrix};$$

see [6]. Note that the first column of H is given by h. Hence, if F_p denotes the discrete Fourier transform (DFT) matrix of size p, then $(F_m \otimes F_n)$ diagonalizes H; see [2]. More specifically, H has the eigendecomposition

$$H = (F_m \otimes F_n)\Lambda(F_m \otimes F_n)^*,$$

where Λ is a diagonal matrix. Furthermore, for a matrix which is block circulant with circulant blocks, its eigenvalues can be easily computed by taking the Fourier transform of its first column; see [2]. That is,

$$diag(\Lambda) = (F_m \otimes F_n)He_1 = (F_m \otimes F_n)h \tag{10}$$

where e_1 is the first unit vector of size mn. Since the convolution $\star$ is commutative, i.e., $h \star u = u \star h$, (1) can also be expressed as $z = U^{true} h^{true} + \eta$ where U^{true} is a blurring matrix associated with u^{true} and has the same structure as in (9).

Note that under the H^1 regularization, the AMHU iteration according to Table 2 can be written as

Given u^0: iterating $k = 0, 1, \ldots$

- Solve for h^{k+1}

$$(U^{k*}U^k - \alpha_2 \triangle)h^{k+1} = U^{k*}z \tag{11}$$

h^{k+1} satisfies periodic boundary condition

- Solve for u^{k+1}

$$(H^{k+1*}H^{k+1} - \alpha_1 \triangle)u^{k+1} = H^{k+1*}z \tag{12}$$

u^{k+1} satisfies periodic boundary condition

where $\nabla_h H^1(h) = -2\triangle h$ and $\nabla_u H^1(u) = -2\triangle u$. Here

$$\triangle = circ_m(-2, 1, 0, \ldots, 0, 1) \otimes I_n + I_m \otimes circ_n(-2, 1, 0, \ldots, 0, 1)$$

is the 2D discrete Laplacian of size mn with periodic boundary condition and $circ_n(c_1, \ldots, c_n)$ denotes an n–by–n circulant matrix with first column $(c_1, \ldots, c_n)^t$.

Note that the matrices U^k, H^k and $\triangle$ in (11) and (12) are block circulant matrices with circulant blocks. By (10), we have the following eigendecompositions:

$$U^k = (F_m \otimes F_n)\Lambda_{U^k}(F_m \otimes F_n)^*,$$

$$H^k = (F_m \otimes F_n)\Lambda_{H^k}(F_m \otimes F_n)^*$$

and

$$\triangle = (F_m \otimes F_n)\Lambda_{\triangle}(F_m \otimes F_n)^*$$

where Λ_{U^k}, Λ_{H^k} and $\Lambda_{\triangle}$ are diagonal matrices with diagonals given by

$$diag(\Lambda_{U^k}) = (F_m \otimes F_n)U^k e_1 = (F_m \otimes F_n)u^k$$

$$diag(\Lambda_{H^k}) = (F_m \otimes F_n)H^k e_1 = (F_m \otimes F_n)h^k$$

and

$$diag(\Lambda_{\triangle}) = \left[-4 + 2\cos\frac{2\pi\xi_x}{m} + 2\cos\frac{2\pi\xi_y}{n}\right]_{\xi_x=0,\ldots m-1, \xi_y=0,\ldots n-1}.$$

The two dimensional indices ξ_x and ξ_y are the frequency variables of the Fourier domain and correspond to the spatial indices p and q. We will call the eigenvalues of U^k, H^k and Δ, the Fourier frequency spectra of u^k, h^k and Δ and will be denoted by

$$\mathcal{U}^k = [\mathcal{U}^k(\xi_x, \xi_y)]_{\xi_x=0,1,\ldots,m-1, \xi_y=0,1,\ldots,n-1} = (F_m \otimes F_n)u^k$$

$$\mathcal{H}^k = [\mathcal{H}^k(\xi_x, \xi_y)]_{\xi_x=0,1,\ldots,m-1, \xi_y=0,1,\ldots,n-1} = (F_m \otimes F_n)h^k \tag{13}$$

and

$$\mathcal{R} = [\mathcal{R}(\xi_x,\xi_y)]_{\xi_x=0,1,\ldots,m-1,\xi_y=0,1,\ldots,n-1} = \left[4 - 2\cos\frac{2\pi\xi_x}{m} - 2\cos\frac{2\pi\xi_y}{n}\right]_{\xi_x=0,\ldots m-1,\xi_y=0,\ldots n-1}.$$

In addition, we define the Fourier spectrum of z to be

$$\mathcal{Z} = [\mathcal{Z}(\xi_x,\xi_y)]_{\xi_x=0,1,\ldots,m-1,\xi_y=0,1,\ldots,n-1} = (F_m \otimes F_n)z.$$

Multiplying $(F_m \otimes F_n)^*$ to equations (11) and (12) and make use of (13), the AMHU algorithm in frequency domain can be expressed as:

Given $\mathcal{U}^0$, iterating $k = 0, 1, \ldots$

$$(14)\qquad \begin{cases} \mathcal{H}^{k+1}(\xi_x,\xi_y) &= \dfrac{\overline{\mathcal{U}^k(\xi_x,\xi_y)}\mathcal{Z}(\xi_x,\xi_y)}{|\mathcal{U}^k(\xi_x,\xi_y)|^2 + \alpha_2\mathcal{R}(\xi_x,\xi_y)} \\ \mathcal{U}^{k+1}(\xi_x,\xi_y) &= \dfrac{\overline{\mathcal{H}^{k+1}(\xi_x,\xi_y)}\mathcal{Z}(\xi_x,\xi_y)}{|\mathcal{H}^{k+1}(\xi_x,\xi_y)|^2 + \alpha_1\mathcal{R}(\xi_x,\xi_y)} \end{cases}.$$

In the following section, we will provide analysis to the discrete AM algorithm.

3. Analysis of the AM algorithm. In this section, we are going to show that the discrete AM algorithm converges. The analysis will be for the case of H^1 regularization. There are four main objectives in this section, namely

1. Prove that AMHU converges and determine the limit to which it converges.
2. Determine whether the restored (u, h) satisfies some of the physical constraints (e.g $\sum_{p,q} h(p,q) = 1$).
3. Discuss some of the possible limitations of using H^1 regularization. In particular, we will discuss why H^1 regularization works reasonably in non-blind deconvolution but not in blind deconvolution, see figure 1.
4. Show that the two algorithms AMUH and AMHU produce the same iterates if the initial guesses h^0 and u^0 are properly initialized and therefore conclude that the AMUH algorithm also converges for any h^0.

In the following, we will show that the discrete AM algorithm (14) converges for any given $\mathcal{U}^0$ and we will determine the limits

$$(15)\qquad \mathcal{U}(\xi_x,\xi_y) \equiv \lim_{k\to\infty}\mathcal{U}^k(\xi_x,\xi_y) \qquad \text{and} \qquad \mathcal{H}(\xi_x,\xi_y) \equiv \lim_{k\to\infty}\mathcal{H}^k(\xi_x,\xi_y).$$

Let us first write the complex number $\mathcal{U}^k(\xi_x,\xi_y)$ as $\mathcal{U}^k(\xi_x,\xi_y) = |\mathcal{U}^k(\xi_x,\xi_y)|e^{i\theta_{\mathcal{U}^k}(\xi_x,\xi_y)}$ where $|\mathcal{U}^k(\xi_x,\xi_y)|$ and $\theta_{\mathcal{U}^k}(\xi_x,\xi_y)$ are usually called the magnitude spectrum and the phase spectrum of u^k. Similarly, we can write $\mathcal{H}^k(\xi_x,\xi_y)$ as $|\mathcal{H}^k(\xi_x,\xi_y)|e^{i\theta_{\mathcal{H}^k}(\xi_x,\xi_y)}$. We will show that both the magnitude spectrum and the phase spectrum of u^k and h^k are going to converge.

THEOREM 3.1. *For a given initial $\mathcal{U}^0(\xi_x,\xi_y)$, the AMHU iteration converges and has limit $(\mathcal{U}(\xi_x,\xi_y),\mathcal{H}(\xi_x,\xi_y))$ given by:*

1. *For those (ξ_x,ξ_y) with $\mathcal{U}^0(\xi_x,\xi_y) = 0$, $(\mathcal{U}(\xi_x,\xi_y),\mathcal{H}(\xi_x,\xi_y)) = (0,0)$.*
2. *For those (ξ_x,ξ_y) with $\mathcal{U}^0(\xi_x,\xi_y) \neq 0$, $(\mathcal{U}(\xi_x,\xi_y),\mathcal{H}(\xi_x,\xi_y))$ is given by*

$$\begin{cases} (\mathcal{U}^0(0,0), \mathcal{Z}(0,0)/\mathcal{U}^0(0,0)) & \text{if } (\xi_x,\xi_y) = (0,0) \\ (0,0) & \text{if } (\xi_x,\xi_y) \neq (0,0) \text{ and } |\mathcal{Z}(\xi_x,\xi_y)|^2 \leq \alpha_1\alpha_2\mathcal{R}(\xi_x,\xi_y)^2 \\ \left(Me^{i\theta_{\mathcal{U}^0}(\xi_x,\xi_y)},\right. & \\ \left.\sqrt{\frac{\alpha_1}{\alpha_2}}Me^{i(\theta_{\mathcal{Z}}(\xi_x,\xi_y)-\theta_{\mathcal{U}^0}(\xi_x,\xi_y))}\right) & \text{if } (\xi_x,\xi_y) \neq (0,0) \text{ and } |\mathcal{Z}(\xi_x,\xi_y)|^2 > \alpha_1\alpha_2\mathcal{R}(\xi_x,\xi_y)^2 \end{cases}$$

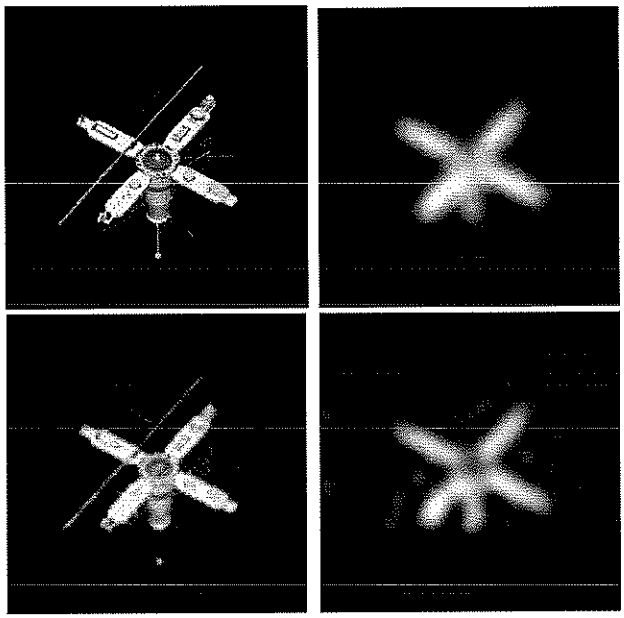

FIG. 1. *Top left: Original image. Top right: Observed image (without noise) Bottom left: The best restored image by nonblind deconvolution using H^1 regularization. Bottom right: The best restored image by blind deconvolution using H^1 regularization.*

where $M = \sqrt{\sqrt{\frac{\alpha_2}{\alpha_1}}|\mathcal{Z}(\xi_x,\xi_y)| - \alpha_2\mathcal{R}(\xi_x,\xi_y)}$.

Proof. Given in the appendix. □

From Theorem 3.1, we can make some interesting observations about the converged solution (u,h). First, the total image intensity is preserved:

$$\mathcal{U}(0,0) = \mathcal{U}^0(0,0) \quad \Longrightarrow \quad \sum_{p=0}^{m-1}\sum_{q=0}^{n-1} u(p,q) = \sum_{p=0}^{m-1}\sum_{q=0}^{n-1} u^0(p,q).$$

Second, if $\alpha_1\alpha_2\mathcal{R}^2(\xi_x,\xi_y) > |\mathcal{Z}(\xi_x,\xi_y)|^2$ is true for some frequency (ξ_x,ξ_y), which means that regularization is too strong, then both the restored $\mathcal{U}$ and $\mathcal{H}$ at that frequency will be zero. Otherwise, a nonzero spectrum is being restored. Theorem 3.1 tells us that the restored phase spectrum satisfies:

$$\theta_{\mathcal{U}}(\xi_x,\xi_y) = \theta_{\mathcal{U}^0}(\xi_x,\xi_y),$$

that is, the phase of the restored image u is invariant. Moreover, the spectra $\mathcal{H}(\xi_x,\xi_y)$ and $\mathcal{U}(\xi_x,\xi_y)$ differ only by a scaling factor $\sqrt{\frac{\alpha_1}{\alpha_2}}$. The above interpretations are now summarized in the following corollaries.

COROLLARY 3.2. *The AMHU converges to a solution (u,h) which satisfies:*

1. **(Total Intensity Preserving)**

$$\sum_{p=0}^{m-1}\sum_{q=0}^{n-1} u(p,q) = \sum_{p=0}^{m-1}\sum_{q=0}^{n-1} u^0(p,q),$$

and

$$\sum_{p=0}^{m-1}\sum_{q=0}^{n-1} h(p,q) = \left(\sum_{p=0}^{m-1}\sum_{q=0}^{n-1} z(p,q)\right) / \left(\sum_{p=0}^{m-1}\sum_{q=0}^{n-1} u^0(p,q)\right).$$

2. **(Phase Invariant)**

$$\theta_{\mathcal{U}} = \theta_{\mathcal{U}^0},$$

$$\theta_{\mathcal{H}} = \theta_{\mathcal{Z}} - \theta_{\mathcal{U}^0}.$$

3. **(Relation on Magnitude)**

$$\mathcal{U}(\xi_x, \xi_y) = \sqrt{\frac{\alpha_2}{\alpha_1}}\mathcal{H}(\xi_x, \xi_y)$$

except when $(\xi_x, \xi_y) = (0, 0)$.

As we mentioned earlier, usually u^0 is chosen to be the observed image z. In this case, Corollary 3.2 tells us that the restored blurring function h will automatically satisfy $\sum_{p=0}^{m-1}\sum_{q=0}^{n-1} h(p,q) = 1$ and $\theta_{\mathcal{H}} = 0$. Note that $\theta_{\mathcal{H}} = 0$ implies that h is an even function. In [3], we explicitly impose the constraints $\sum_{p=0}^{m-1}\sum_{q=0}^{n-1} h(p,q) = 1$ and h is even, by performing the projection $h^k \leftarrow h^k / \sum h^k$, $h^k(x,y) \leftarrow (h^k(x,y) + h^k(-x,-y))/2$ in each AM step. Our results here show that these were not necessary.

COROLLARY 3.3. *If* $u^0 = z$, *then AMHU converges to solution* (u, h) *which satisfies:*

1. **(Total Intensity Preserving)**

$$\sum_{p=0}^{m-1}\sum_{q=0}^{n-1} u(p,q) = \sum_{p=0}^{m-1}\sum_{q=0}^{n-1} u^{true}(p,q)$$

and

$$\sum_{p=0}^{m-1}\sum_{q=0}^{n-1} h(p,q) = 1.$$

2. **(Phase Invariant)**

$$\theta_{\mathcal{U}} = \theta_{\mathcal{Z}},$$

$$\theta_{\mathcal{H}} = 0, \qquad i.e., \ \ h \ \ is \ \ even.$$

3. **(Relation on Magnitude)**

$$|\mathcal{U}(\xi_x, \xi_y)| = \sqrt{\frac{\alpha_2}{\alpha_1}}|\mathcal{H}(\xi_x, \xi_y)|$$

except when $(\xi_x, \xi_y) = (0, 0)$.

From Theorem 3.1, Corollaries 3.2 and 3.3, we observe that there are some possible limitations of using the H^1 regularization with the AMHU algorithm:

1. Corollary 3.2 tells us that $\theta_{\mathcal{U}} = \theta_{\mathcal{U}^0}$, which implies that the AMHU algorithm preserves the phase of the initial guess u^0. However, $\theta_{\mathcal{U}^0} \neq \theta_{\mathcal{U}^{true}}$ in general. One typical situation is when $u^0 = z$ which has Fourier transform given by

$$\mathcal{Z} = \mathcal{H}^{true}\mathcal{U}^{true} + \mathcal{N}$$

where $\mathcal{U}^{true}$, $\mathcal{H}^{true}$ and $\mathcal{N}$ are the discrete 2D Fourier transforms of u^{true}, h^{true} and η respectively. In the absence of noise, i.e., $\mathcal{N} = 0$, we have $\theta_{\mathcal{Z}} = \theta_{\mathcal{H}^{true}} + \theta_{\mathcal{U}^{true}}$ which implies that the blur may change the phase of $\mathcal{U}^{true}$ (e.g. when h^{true} is a motion blur or out of focus blur) unless $\theta_{\mathcal{H}^{true}} = 0$ (e.g. when h^{true} is a Gaussian then $\mathcal{H}^{true}$ is also a Gaussian which is positive and hence $\theta_{\mathcal{H}^{true}} = 0$). It is obvious that the presence of noise will change the phase of the original image and make $\theta_{\mathcal{Z}}$ different from $\theta_{\mathcal{U}^{true}}$. We will demonstrate in §3 that this will lead to a less satisfactory restoration.

2. If we start the AMHU algorithm with $u^0 = z$, then the restored h is always an even function which may be a limitation if the true h is not even.
3. The magnitude spectrum of the restored blurring function h differs by only a scaling factor from that of the restored image u. More precisely, for any $(\xi_x, \xi_y) \neq (0,0)$, $|\mathcal{U}(\xi_x, \xi_y)| = C|\mathcal{H}(\xi_x, \xi_y)|$ where $C = \sqrt{\frac{\alpha_2}{\alpha_1}}$ is a constant *independent* on ξ_x, ξ_y. However in practice, $\mathcal{U}^{true}$ and $\mathcal{H}^{true}$ rarely follows such a relation.

We stress that the situation is much worse than in the case of non-blind deconvolution. In that case, the restored u is given by

$$\mathcal{U}(\xi_x, \xi_y) = \frac{\overline{\mathcal{H}^{true}(\xi_x, \xi_y)}\mathcal{Z}(\xi_x, \xi_y)}{|\mathcal{H}^{true}(\xi_x, \xi_y)|^2 + \alpha\mathcal{R}(\xi_x, \xi_y)},$$

where α is the regularization parameter. In the case noise is absent, $\mathcal{Z} = \mathcal{H}^{true}\mathcal{U}^{true}$. Hence,

$$\mathcal{U}(\xi_x, \xi_y) = \frac{|\mathcal{H}^{true}(\xi_x, \xi_y)|^2}{|\mathcal{H}^{true}(\xi_x, \xi_y)|^2 + \alpha\mathcal{R}(\xi_x, \xi_y)}\mathcal{U}^{true}(\xi_x, \xi_y).$$

This means the restored u has the same phase spectrum as the original image. The magnitude spectrum of u is basically the same as that of u^{true} except it is slightly scaled down by the factor $\frac{|\mathcal{H}^{true}|^2}{|\mathcal{H}^{true}|^2 + \alpha\mathcal{R}}$ which is close to one as α is usually very small when noise is zero. This explains why the restored u by nonblind deconvolution with H^1 regualarization is much better than that by blind deconvolution. In conclusion, H^1 regularization may produce less satisfactory restoration result in non-blind deconvolution.

Next, we will show that the AMHU algorithm is equivalent to the AMUH algorithm in the sense that AMHU algorithm with initial guess u^0 will produce the same iterates as AMUH if h^0 is properly initialized and vice versa. First the AMUH algorithm can be expressed in frequecny domain as:
Given $\mathcal{H}^0$, iterating $n = 0, 1, \ldots$

$$\text{(16)} \qquad \begin{cases} \mathcal{U}^{k+1}(\xi_x, \xi_y) &= \dfrac{\overline{\mathcal{H}^k(\xi_x, \xi_y)}\mathcal{Z}(\xi_x, \xi_y)}{|\mathcal{H}^k(\xi_x, \xi_y)|^2 + \alpha_1\mathcal{R}(\xi_x, \xi_y)} \\ \mathcal{H}^{k+1}(\xi_x, \xi_y) &= \dfrac{\overline{\mathcal{U}^{k+1}(\xi_x, \xi_y)}\mathcal{Z}(\xi_x, \xi_y)}{|\mathcal{U}^{k+1}(\xi_x, \xi_y)|^2 + \alpha_2\mathcal{R}(\xi_x, \xi_y)} \end{cases}.$$

We are going to show that AMUH and AMHU produce the same iterates if we started with appropriate initial guesses. Let $(\mathcal{U}^k_{HU}(\xi_x, \xi_y), \mathcal{H}^k_{HU}(\xi_x, \xi_y))$ and $(\mathcal{U}^k_{UH}(\xi_x, \xi_y), \mathcal{H}^k_{UH}(\xi_x, \xi_y))$ be the iterates generated by the AMHU and AMUH algorithms respectively. Then it

is not difficult to check that the AMHU algorithm with initial guess $\mathcal{U}^0_{HU}$ generates the same iterates as the AMUH algorithm with the initial guess

$$\mathcal{H}^0_{UH}(\xi_x,\xi_y) = \frac{\overline{\mathcal{U}^0_{HU}(\xi_x,\xi_y)}\mathcal{Z}(\xi_x,\xi_y)}{|\mathcal{U}^0_{HU}(\xi_x,\xi_y)|^2 + \alpha_2\mathcal{R}(\xi_x,\xi_y)}. \tag{17}$$

More precisely, we have the following lemma.

LEMMA 3.4. *If AMHU starts with initial guess $\mathcal{U}^0_{HU}$ and AMUH starts with initial guess defined in (17), then*

$$\mathcal{U}^k_{HU} = \mathcal{U}^k_{UH} \qquad \text{and} \qquad \mathcal{H}^k_{HU} = \mathcal{H}^{k-1}_{UH}$$

for $n = 1, 2, \ldots,$.

Since at each AM step, AMUH produces the same iterate as AMHU, obviously AMUH converges. For the sake of completeness, we state the following theorem.

THEOREM 3.5. *For a given initial $\mathcal{H}^0(\xi_x,\xi_y)$, the AMUH algorithm converges and has limit $(\mathcal{U}(\xi_x,\xi_y),\mathcal{H}(\xi_x,\xi_y))$ given by*

1. *For those (ξ_x,ξ_y) with $\mathcal{H}^0(\xi_x,\xi_y) = 0$, $(\mathcal{U}(\xi_x,\xi_y),\mathcal{H}(\xi_x,\xi_y)) = (0,0)$.*
2. *For those (ξ_x,ξ_y) with $\mathcal{H}^0(\xi_x,\xi_y) \neq 0$, $(\mathcal{U}(\xi_x,\xi_y),\mathcal{H}(\xi_x,\xi_y))$ is given by*

$$\begin{cases} (\mathcal{Z}(0,0)/\mathcal{H}^0(0,0), \mathcal{H}^0(0,0)) & \text{if } (\xi_x,\xi_y) = (0,0) \\ (0,0) & \text{if } (\xi_x,\xi_y) \neq (0,0) \text{ and } |\mathcal{Z}(\xi_x,\xi_y)|^2 \leq \alpha_1\alpha_2\mathcal{R}(\xi_x,\xi_y)^2 \\ \left(Me^{i(\theta_{\mathcal{Z}}(\xi_x,\xi_y)-\theta_{\mathcal{H}^0}(\xi_x,\xi_y))},\right. & \\ \left.\sqrt{\frac{\alpha_1}{\alpha_2}}Me^{i\theta_{\mathcal{H}^0}(\xi_x,\xi_y)}\right) & \text{if } (\xi_x,\xi_y) \neq (0,0) \text{ and } |\mathcal{Z}(\xi_x,\xi_y)|^2 > \alpha_1\alpha_2\mathcal{R}(\xi_x,\xi_y)^2 \end{cases}$$

where $M = \sqrt{\sqrt{\frac{\alpha_2}{\alpha_1}}|\mathcal{Z}(\xi_x,\xi_y)| - \alpha_2\mathcal{R}(\xi_x,\xi_y)}$.

Notice that the limiting spectrum $\mathcal{U}(\xi_x,\xi_y)$ and $\mathcal{H}(\xi_x,\xi_y)$ will depend on $\mathcal{H}^0(\xi_x,\xi_y)$ instead of $\mathcal{U}^0(\xi_x,\xi_y)$.

4. Numerical experiments. In this section, we will verify the theory developed in §3. Namely, if we start with $u^0 = z$, then the restored h is even, $\sum_{p=0}^{m-1}\sum_{q=0}^{n-1} h(p,q) = 1$ and $|\mathcal{H}(\xi)| = \sqrt{\alpha_1/\alpha_2}|\mathcal{U}(\xi)|$ except $\xi = 0$. We will also show that the theory for the periodic boundary condition provides a good prediction for the Neumann boundary condition case which we actually used in practice. For the ease of presenting the spectra of the restored image and blurring function, our experiements will be all in one dimension and the frequency variable is denoted by ξ. We remark that in our experiments, we have examined various regularization parameters α_1 and α_2 and we report the best restored signal (the one with the largest impoved signal to noise ratio (ISNR)) for each case.

In figures 2 – 4, we show the original signal, the PSF and the blurred image in both spatial and frequency domains. The blurring function in this experiment is a motion blur PSF which is even, and has $\sum_{p=0}^{m-1}\sum_{q=0}^{n-1} h^{true}(p,q) \equiv \mathcal{H}^{true}(0) = 1$, see figure 3. In figures 5 – 6, we show the restored u and h by using the AMHU algorithm with periodic boundary condition. We observed that the restored h is even and $\mathcal{H}(0)$ is exactly equal to one which means that the restored h satisfies $\sum_{p=0}^{m-1}\sum_{q=0}^{n-1} h(p,q) = 1$ which agrees with $\sum_{p=0}^{m-1}\sum_{q=0}^{n-1} h^{true}(p,q) = 1$ in this experiment. Furthermore, in figure 7, we plot $|\mathcal{H}(\xi)|$ and $\sqrt{\alpha_1/\alpha_2}|\mathcal{U}(\xi)|$. It shows that the relation $|\mathcal{H}(\xi)| = \sqrt{\alpha_1/\alpha_2}|\mathcal{U}(\xi)|$ holds

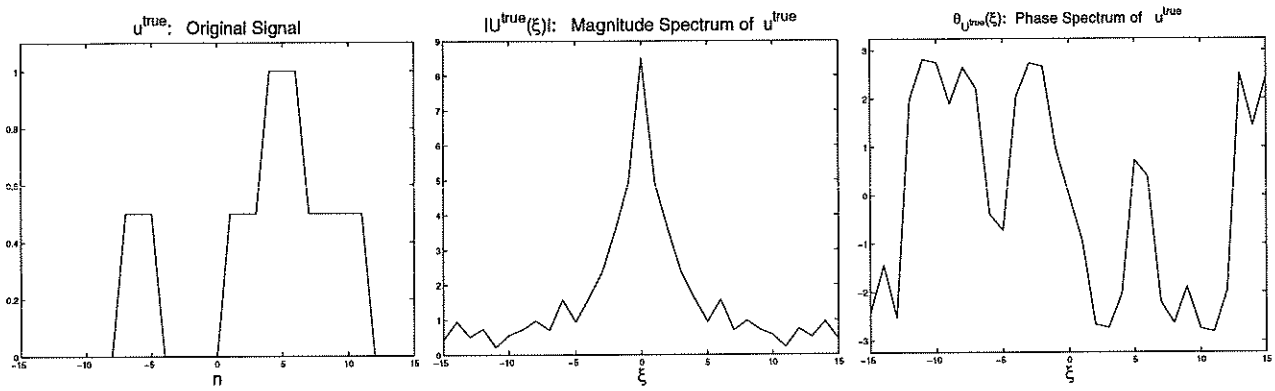

FIG. 2. *Original signal u^{true} (left), its magnitude spectrum $|\mathcal{U}^{true}(\xi)|$ (middle) and its phase spectrum $\theta_{\mathcal{U}^{true}}$ (right)*

except when $\xi = 0$. However, $|\mathcal{H}^{true}(\xi)|$ and $\sqrt{\alpha_1/\alpha_2}|\mathcal{U}^{true}(\xi)|$ do not satisfy the relation.

Figure 8 shows the result for nonblind deconvolution, i.e., given h^{true} and z, we try to restore u^{true}. The restored u looks almost the same as the original signal and has almost the same phase and magnitude spectra as the original signal.

In conclusion, H^1 produces less satisfactory restoration result in blind deconvolution which is because it does not correct the phase of u^0 and the restored u and h are enforced to satisfy $|\mathcal{H}(\xi)| = \sqrt{\alpha_1/\alpha_2}|\mathcal{U}(\xi)|$ which may not be true for the true image and PSF.

In figures 9 – 10, we show the spectra of the restored image and the identified PSF when Neumann boundary condition is imposed. In this case, the restored u and h at the boundary are smoother than those for the periodic boundary condition. Also we note that the phase spectra of u and h are almost the same as those restored under the periodic boundary condition. Hence we conclude that the Fourier analysis for the periodic case provides a very good prediction for that of the Neumann boundary condition.

Even though the AM algorithm with H^1 regularization has limitation on restoring the magnitude and phase spectra of u^{true} and h^{true}, the AM algorithm with TV regularization seems to work very well, see [3]. In figures 11 – 12, we show the spectra of the restored image and the identified PSF for TV regularization when Neumann boundary condition is imposed. We observed that both the phase and magnitude spectra of u and h are restored almost exactly. However, due to the highly nonlinear property of TV regularization, we do not have any analysis for blind TV restoration yet.

5. Appendix: Proof for Theorem 3.1. To prove the theorem, we are going to show that both the magnitude spectrum and the phase spectrum of u^k and h^k are going to converge. The following lemma proves that the phase spectrum converges.

LEMMA 5.1. *The AMHU algorithm produces (u^k, h^k) satisfies*

$$\theta_{\mathcal{U}^k}(\xi_x, \xi_y) = \theta_{\mathcal{U}^{k-1}}(\xi_x, \xi_y) = \theta_{\mathcal{U}^0}(\xi_x, \xi_y)$$

and

$$\theta_{\mathcal{H}^{k+1}}(\xi_x, \xi_y) = \theta_{\mathcal{H}^k}(\xi_x, \xi_y) = \theta_{\mathcal{Z}}(\xi_x, \xi_y) - \theta_{\mathcal{U}^0}(\xi_x, \xi_y)$$

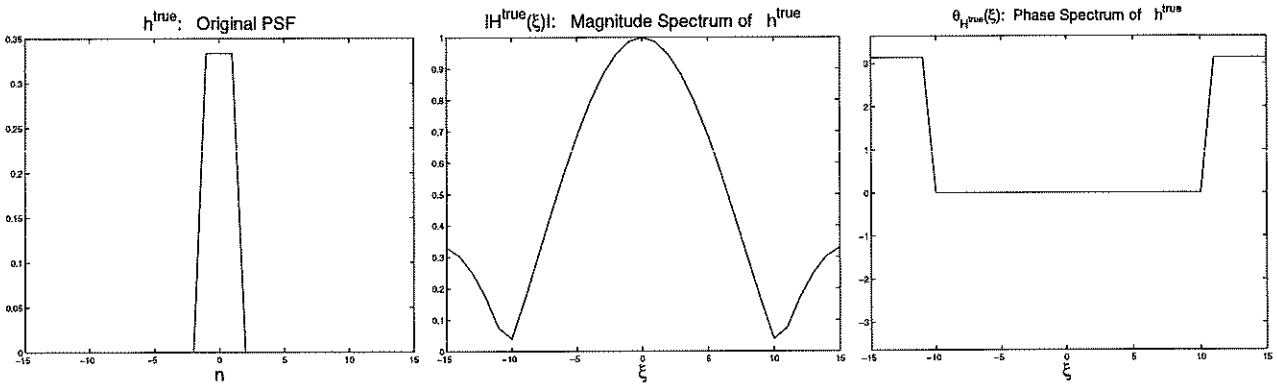

FIG. 3. *Original PSF h^{true} (left) which is a motion blur, its magnitude spectrum $|\mathcal{H}^{true}(\xi)|$ (middle) and its phase spectrum $\theta_{\mathcal{H}^{true}}$ (right). Motion blur has non-zero phase spectrum which implies that $\theta_{\mathcal{Z}} \neq \theta_{\mathcal{U}^{true}}$, see Fig 4.*

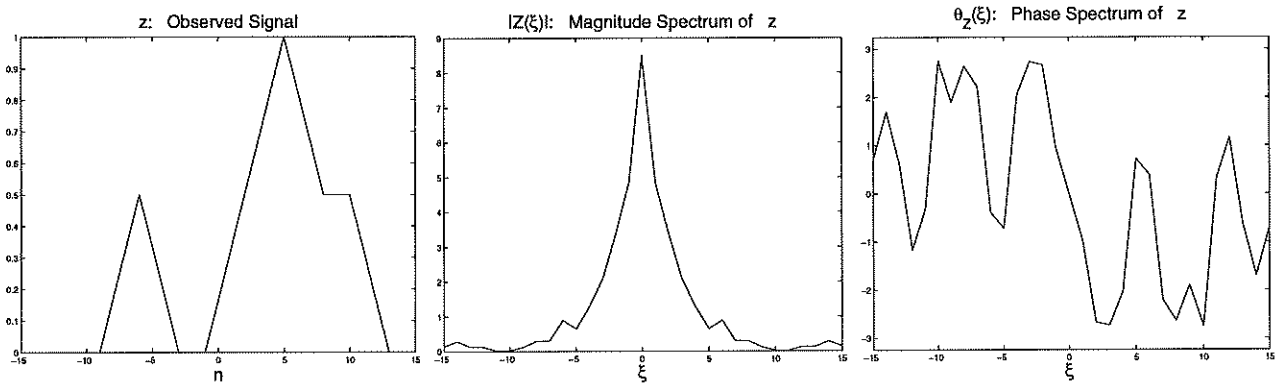

FIG. 4. *Observed signal z without noise (left), its magnitude spectrum (middle) $|\mathcal{Z}(\xi)|$ and its phase spectrum $\theta_{\mathcal{Z}}$ (right). Note that since noise = 0, $|\mathcal{Z}(\xi)| = |\mathcal{U}^{true}(\xi)| \cdot |\mathcal{H}^{true}(\xi)|$ and in this case $\theta_{\mathcal{Z}} = \theta_{\mathcal{U}^{true}} + \theta_{\mathcal{H}^{true}}$.*

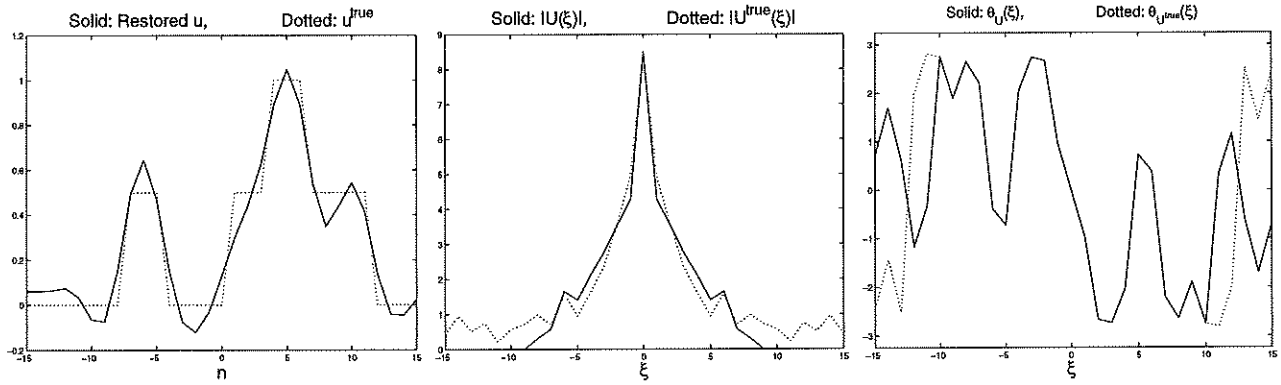

FIG. 5. *Restored signal (solid line) u by H^1 regularization (left), its magnitude spectrum $|\mathcal{U}(\xi)|$ (middle) and its phase spectrum $\theta_{\mathcal{U}}$ (right). These plots are interlaced with the original signal and its spectra by dotted line.*

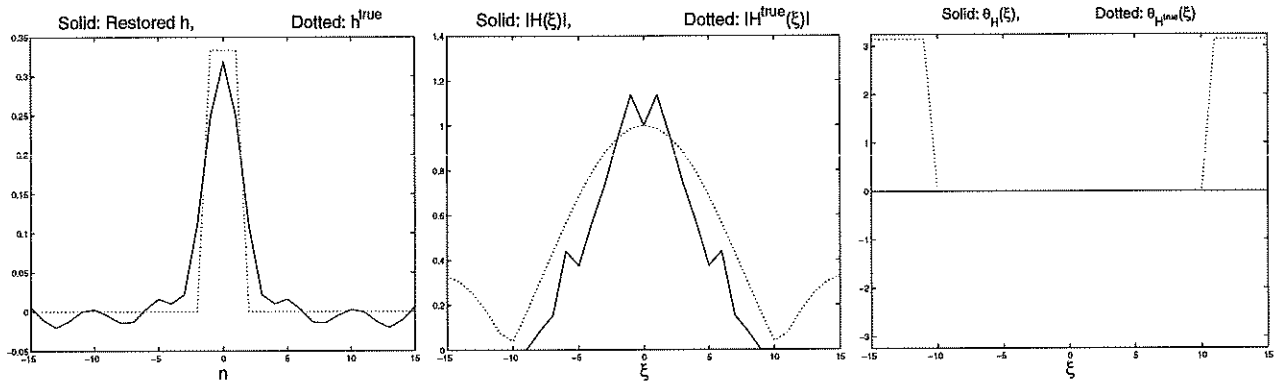

FIG. 6. *Restored blurring function (solid line) h by H^1 regularization (left), its magnitude spectrum $|\mathcal{H}(\xi)|$ (middle) and its phase spectrum $\theta_{\mathcal{H}}$ (right). These plots are interlaced with the true PSF and its spectra by dotted line. Observation: For $u^0 = z$, $\theta_{\mathcal{H}}$ is always zero. That is the restored h must be an even function.*

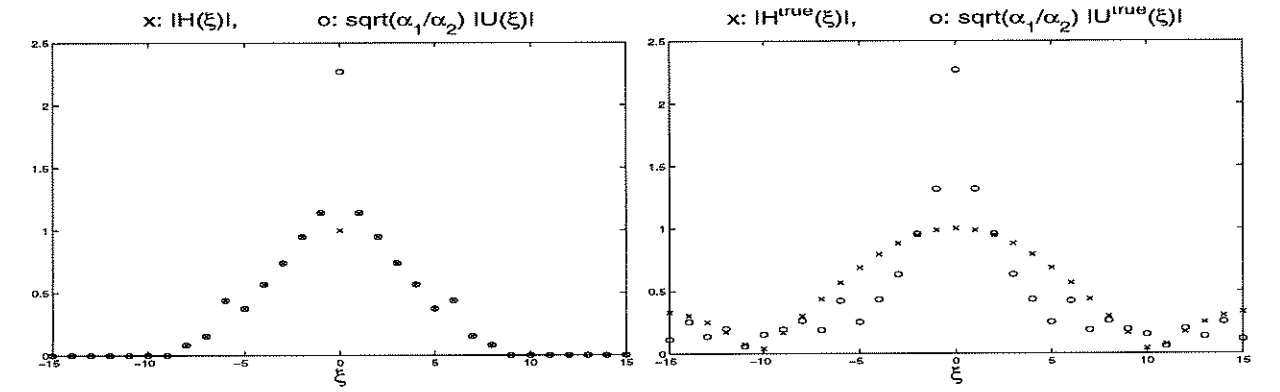

FIG. 7. *Comparison of the magnitude spectrum of the restored u and h by H^1 regularization. Left: we plot $|\mathcal{H}(\xi)|$ (denoted by $\times$) and $\sqrt{\alpha_1/\alpha_2}|\mathcal{U}(\xi)|$ (denoted by o). Observation: $|\mathcal{H}(\xi)| = \sqrt{\alpha_1/\alpha_2}|\mathcal{U}(\xi)|$ except when $\xi = 0$. Right: $\mathcal{H}^{true}$ and $\mathcal{U}^{true}$ do not follow this relation.*

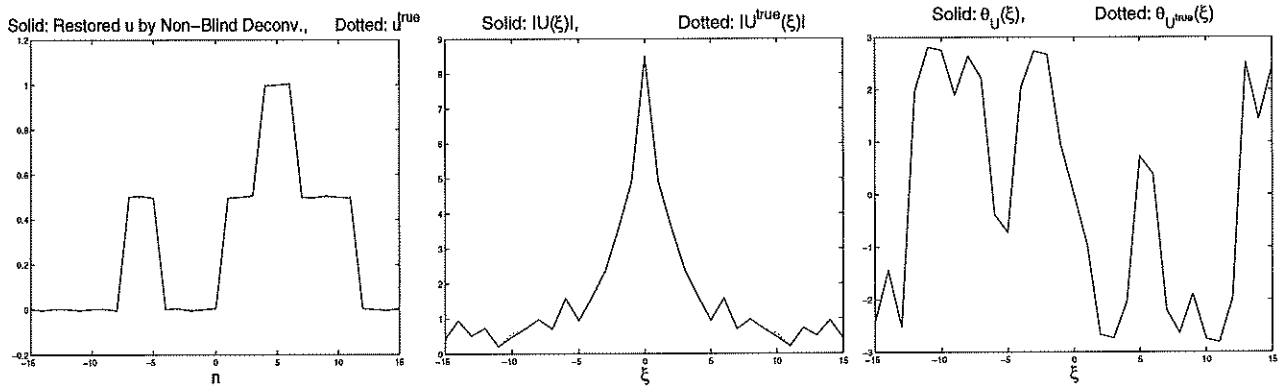

FIG. 8. *Restored u (left) by nonblind deconvolution with H^1 regularization, its magnitude spectrum (middel) and phase spectrum (right). These plots are interlaced with the original signal and its spectra by dotted line. H^1 regularization restores almost exactly the original signal.*

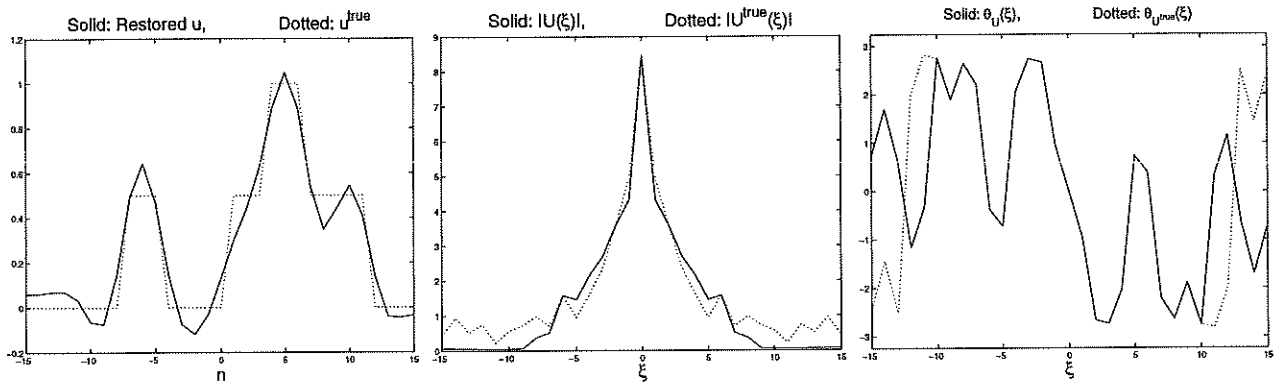

FIG. 9. *Restored signal (solid line) u by H^1 regularization (left) with Neumann BC, its magnitude spectrum $|\mathcal{U}(\xi)|$ (middle) and its phase spectrum $\theta_{\mathcal{U}}$ (right). These plots are interlaced with the original signal and its spectra by dotted line.*

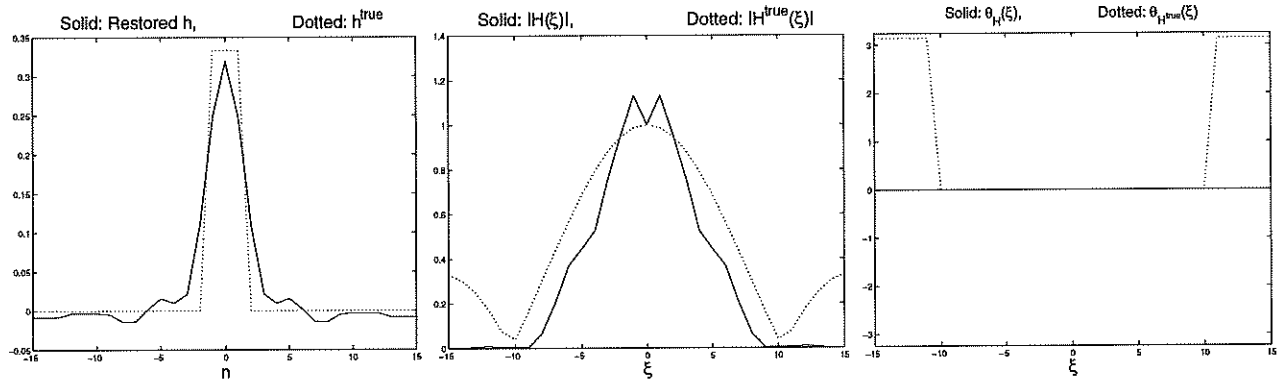

FIG. 10. *Restored blurring function (solid line) h by H^1 regularization (left) with Neumann BC, its magnitude spectrum $|\mathcal{H}(\xi)|$ (middle) and its phase spectrum $\theta_{\mathcal{H}}$ (right). These plots are interlaced with the true PSF and its spectra by dotted line. Observation: $\theta_{\mathcal{H}} = 0$ which indicates that the theorectical results for periodic boundary condition predict the results for Neumann boundary condition.*

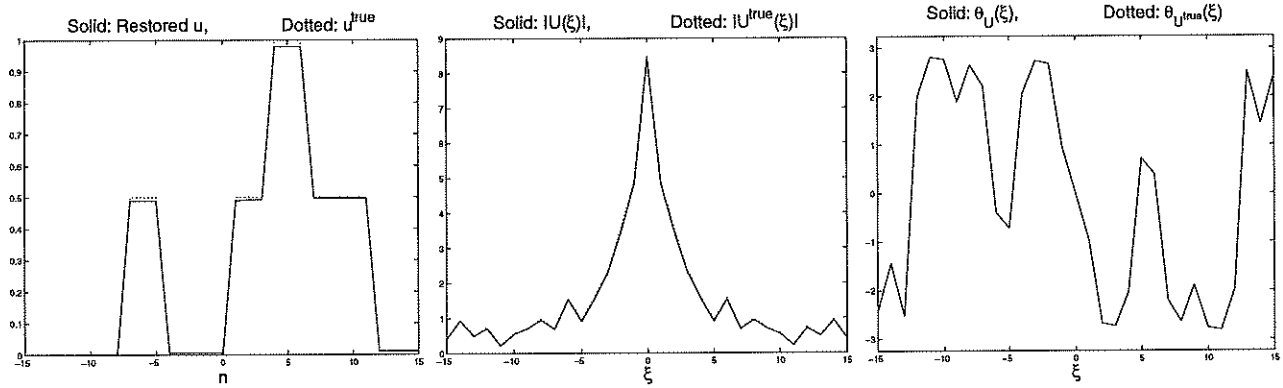

FIG. 11. *Restored signal (solid line) u by TV regularization (left) with Neumann BC, its magnitude spectrum $|\mathcal{U}(\xi)|$ (middle) and its phase spectrum $\theta_{\mathcal{U}}$ (right). These plots are interlaced with the original signal and its spectra by dotted line. Observation: unlike the AM algorithm with H^1 regularization, the AM algorithm with TV regularization restores a much better restored image.*

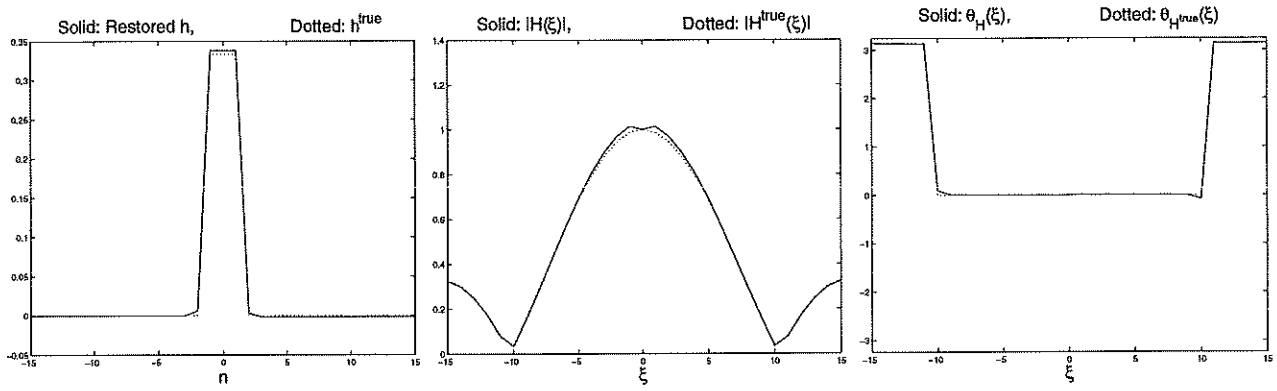

FIG. 12. *Restored blurring function (solid line) h by TV regularization (left) with Neumann BC, its magnitude spectrum $|\mathcal{H}(\xi)|$ (middle) and its phase spectrum $\theta_{\mathcal{H}}$ (right). These plots are interlaced with the true PSF and its spectra by dotted line. Observation: unlike the H^1 regularization which always restores a zero phase spectrum (see Fig 6), TV regularization can recover the phase spectrum of the original PSF.*

for $n = 1, 2, \ldots$. In particular, the phase spectrum $\theta_{\mathcal{U}^k}(\xi_x, \xi_y)$ and $\theta_{\mathcal{H}^k}(\xi_x, \xi_y)$ converge and has limits given by $\theta_{\mathcal{U}}(\xi_x, \xi_y) = \theta_{\mathcal{U}^0}(\xi_x, \xi_y)$ and $\theta_{\mathcal{H}}(\xi_x, \xi_y) = \theta_{\mathcal{Z}}(\xi_x, \xi_y) - \theta_{\mathcal{U}^0}(\xi_x, \xi_y)$ respectively.

Proof. According to (14), we have the relations

$$\theta_{\mathcal{H}^{k+1}}(\xi_x, \xi_y) = \theta_{\mathcal{Z}}(\xi_x, \xi_y) - \theta_{\mathcal{U}^k}(\xi_x, \xi_y), \qquad \theta_{\mathcal{U}^{k+1}}(\xi_x, \xi_y) = \theta_{\mathcal{Z}}(\xi_x, \xi_y) - \theta_{\mathcal{H}^{k+1}}(\xi_x, \xi_y)$$

for $n = 0, 1, \ldots$. By making substituion,

$$\theta_{\mathcal{H}^{k+1}}(\xi_x, \xi_y) = \theta_{\mathcal{H}^k}(\xi_x, \xi_y), \qquad \theta_{\mathcal{U}^k}(\xi_x, \xi_y) = \theta_{\mathcal{U}^{k-1}}(\xi_x, \xi_y)$$

for $n = 1, 2, \ldots$. Then results follow immediately. □

Next, we prove that the magnitude spectra $|\mathcal{U}^k(\xi_x, \xi_y)|$ and $|\mathcal{H}^k(\xi_x, \xi_y)|$ also converge.

LEMMA 5.2. *For a given initial $\mathcal{U}^0(\xi_x, \xi_y)$, the sequence $(|\mathcal{U}^k(\xi_x, \xi_y)|, |\mathcal{H}^k(\xi_x, \xi_y)|)$ converges for any frequency (ξ_x, ξ_y) and has limit $(|\mathcal{U}(\xi_x, \xi_y)|, |\mathcal{H}(\xi_x, \xi_y)|)$ given by*

1. *For those (ξ_x, ξ_y) with $\mathcal{U}^0(\xi_x, \xi_y) = 0$, $(\mathcal{U}(\xi_x, \xi_y), \mathcal{H}(\xi_x, \xi_y)) = (0, 0)$.*
2. *For those (ξ_x, ξ_y) with $\mathcal{U}^0(\xi_x, \xi_y) \neq 0$, $(|\mathcal{U}(\xi_x, \xi_y)|, |\mathcal{H}(\xi_x, \xi_y)|)$ is given by*

$$\begin{cases} (|\mathcal{U}^0(0,0)|, |\mathcal{Z}(0,0)|/|\mathcal{U}^0(0,0)|) & \text{if } (\xi_x, \xi_y) = (0,0) \\ (0,0) & \text{if } (\xi_x, \xi_y) \neq (0,0) \text{ and } |\mathcal{Z}(\xi_x, \xi_y)|^2 \leq \alpha_1 \alpha_2 \mathcal{R}(\xi_x, \xi_y)^2 \\ \left(M, \sqrt{\frac{\alpha_1}{\alpha_2}} M\right) & \text{if } (\xi_x, \xi_y) \neq (0,0) \text{ and } |\mathcal{Z}(\xi_x, \xi_y)|^2 > \alpha_1 \alpha_2 \mathcal{R}(\xi_x, \xi_y)^2 \end{cases}$$

where $M = \sqrt{\sqrt{\frac{\alpha_2}{\alpha_1}} |\mathcal{Z}(\xi_x, \xi_y)| - \alpha_2 \mathcal{R}(\xi_x, \xi_y)}$.

Proof. The proof for part 1 directly follows from (14). To prove part 2, let us first introduce some notations. Denote $x_n = |\mathcal{H}^k(\xi_x, \xi_y)|$, $y_n = |\mathcal{U}^k(\xi_x, \xi_y)|$, $z = |\mathcal{Z}(\xi_x, \xi_y)|$ and $r = \mathcal{R}(\xi_x, \xi_y)$. By (14), we have

$$x_{n+1} = \frac{y_n z}{|y_n|^2 + \alpha_2 r} \qquad \text{and} \qquad y_{n+1} = \frac{x_{n+1} z}{|x_{n+1}|^2 + \alpha_1 r}.$$

Eliminating y_n, we obtain a fixed point formula $x_{n+1} = F(x_n)$ where $F : [0,\infty) \to [0,\infty)$ and is given by

$$F(x) = \frac{xz^2(x^2+\alpha_1 r)}{x^2z^2 + \alpha_2 r(x^2+\alpha_1 r)^2}. \tag{18}$$

We will show that the fixed point iteration $x_{n+1} = F(x_n)$ converges for any initial x_0 (i.e., any $\mathcal{H}^0(\xi_x, \xi_y)$). We will study this in three separate cases.

Case (i): $z^2 < \alpha_1\alpha_2 r^2$

It is not difficult to check that in this case $x = F(x)$ has only $x = 0$ as the fixed point. We are going to show that F is a contractive mapping by checking $|F'(x)| < 1$. By (18),

$$\begin{aligned}
|F'(x)| &= \frac{z^2|x^2-\alpha_1 r|}{x^2z^2+\alpha_2 r(x^2+\alpha_1 r)^2} \cdot \frac{|x^2z^2 - \alpha_2 r(x^2+\alpha_1 r)^2|}{x^2z^2+\alpha_2 r(x^2+\alpha_1 r)^2} \\
&< \frac{z^2|x^2-\alpha_1 r|}{\alpha_2 r(x^2+\alpha_1 r)^2} \\
&= \frac{z^2}{\alpha_2 r|x^2+\alpha_1 r|} \cdot \frac{|x^2-\alpha_1 r|}{x^2+\alpha_1 r} \\
&< \frac{z^2}{\alpha_2 r(x^2+\alpha_1 r)} \\
&< \frac{z^2}{\alpha_2\alpha_1 r^2} < 1
\end{aligned}$$

Therefore, F is contractive on $[0,\infty)$. Hence, $x_{n+1} = F(x_n)$ converges to $x = 0$ for any initial guess x_0.

Case (ii): $\alpha_1\alpha_2 r^2 < z^2 < 4\alpha_1\alpha_2 r^2$

In this case, it is not difficult to check that the function F has two fixed points, 0 and $\sqrt{\sqrt{\frac{\alpha_1}{\alpha_2}}z - \alpha_1 r}$. We will show that the iteration $x_{n+1} = F(x_n)$ converges to the fixed point $\sqrt{\sqrt{\frac{\alpha_1}{\alpha_2}}z - \alpha_1 r}$ for any initial $x_0 > 0$. The only time that the iteration converges to 0 is when $x_0 = 0$. Notice that in this case F is not a contractive mapping on $[0,\infty)$ as in Case (i) and makes the proof a little bit tedious. First, let us have some observation and understanding about the function F. A typical function F for this case is presented in figure 13.

(a) The only stationary point of F is a maximum which attains at $x = \sqrt{r\alpha_1}$ and it is larger than the fixed point, i.e.,

$$\sqrt{\sqrt{\frac{\alpha_1}{\alpha_2}}z - \alpha_1 r} < \sqrt{\alpha_1 r}.$$

(b) On $(0, \sqrt{\sqrt{\frac{\alpha_1}{\alpha_2}}z - \alpha_1 r})$, F is increasing and $F(x) > x$.

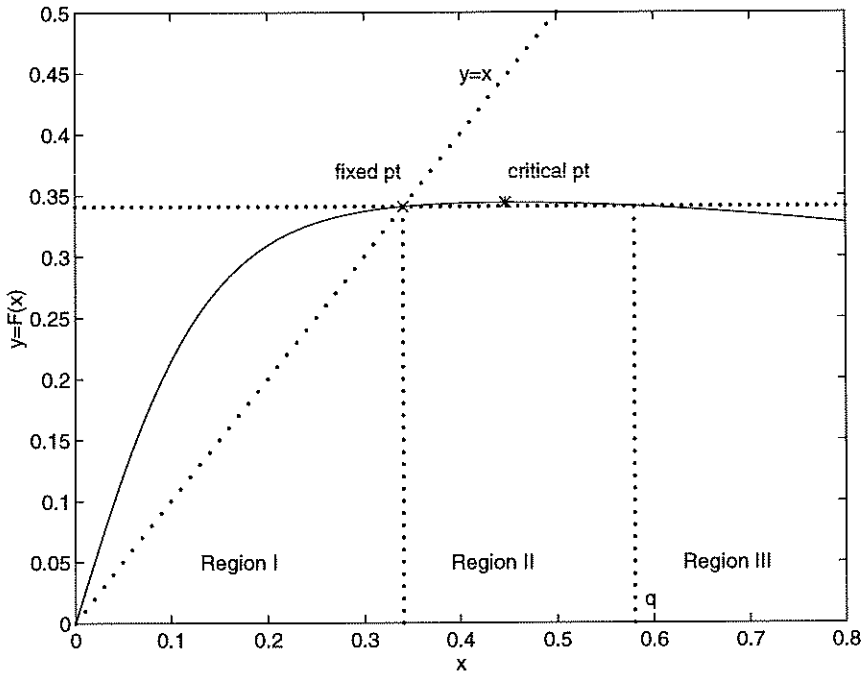

FIG. 13. *Typical F(x) when* $\alpha_1\alpha_2 r^2 < z^2 < 4\alpha_1\alpha_2 r^2$

(c) On $(\sqrt{\sqrt{\frac{\alpha_1}{\alpha_2}}z - \alpha_1 r}, \sqrt{\alpha_1 r})$, F is increasing and $F(\sqrt{r\alpha_1}) < \sqrt{r\alpha_1}$. Hence F maps $[\sqrt{\sqrt{\frac{\alpha_1}{\alpha_2}}z - \alpha_1 r}, \sqrt{\alpha_1 r}]$ into itself.

(d) On $(\sqrt{\alpha_1 r}, \infty)$, F is decreasing.

(e) For any $x > \sqrt{\sqrt{\frac{\alpha_1}{\alpha_2}}z - \alpha_1 r}$, we have

$$|F'(x)| < \frac{z^2|x^2 - \alpha_1 r|}{x^2 z^2 + \alpha_2 r(x^2 + \alpha_1 r)^2} < \frac{z^2|x^2 - \alpha_1 r|}{x^2 z^2 + \alpha_2 r\frac{\alpha_1}{\alpha_2}z^2} = \frac{|x^2 - \alpha_1 r|}{x^2 + \alpha_1 r} < 1.$$

Let $q > \sqrt{r\alpha_1}$ be such that $F(q) = \sqrt{\sqrt{\frac{\alpha_1}{\alpha_2}}z - \alpha_1 r}$. Then $F : [\sqrt{\sqrt{\frac{\alpha_1}{\alpha_2}}z - \alpha_1 r}, q] \longrightarrow [\sqrt{\sqrt{\frac{\alpha_1}{\alpha_2}}z - \alpha_1 r}, q]$ and is contractive.

Now, if the initial guess x_0 lies in Region 1 (see figure 1), i.e., $x_0 \in (0, \sqrt{\sqrt{\frac{\alpha_1}{\alpha_2}}z - \alpha_1 r})$ in which F is increasing and $F : [0, \sqrt{\sqrt{\frac{\alpha_1}{\alpha_2}}z - \alpha_1 r}] \to [0, \sqrt{\sqrt{\frac{\alpha_1}{\alpha_2}}z - \alpha_1 r}]$. Hence, the sequence $x_n = F(x_{n-1})$ is increasing and bounded above by the fixed point $\sqrt{\sqrt{\frac{\alpha_1}{\alpha_2}}z - \alpha_1 r}$. Therefore, the limit $\lim x_n$ exists, denoted it by w. Then $w = F(w)$ which implies that $w = 0$ or $\sqrt{\sqrt{\frac{\alpha_1}{\alpha_2}}z - \alpha_1 r}$. Since the sequence x_n is increasing and $x_0 > 0$ (recall in part 2, we have $|\mathcal{U}^0(f)| > 0$), we have $w = \sqrt{\sqrt{\frac{\alpha_1}{\alpha_2}}z - \alpha_1 r}$.

If x_0 is in Region II, $[\sqrt{\sqrt{\frac{\alpha_1}{\alpha_2}}z - \alpha_1 r}, q]$, then x_n converges because F is contractive on $F : [\sqrt{\sqrt{\frac{\alpha_1}{\alpha_2}}z - \alpha_1 r}, q]$. Since $\sqrt{\sqrt{\frac{\alpha_1}{\alpha_2}}z - \alpha_1 r}$ is the only fixed point on the interval $[\sqrt{\sqrt{\frac{\alpha_1}{\alpha_2}}z - \alpha_1 r}, q]$, x_n converges to $\sqrt{\sqrt{\frac{\alpha_1}{\alpha_2}}z - \alpha_1 r}$.

If x_0 is in Region III, (q, ∞), then $x_1 = F(x_0) < F(q) = \sqrt{\sqrt{\frac{\alpha_1}{\alpha_2}}z - \alpha_1 r}$ because F is decreasing on (q, ∞). Therefore, $x_1 \in (0, \sqrt{\sqrt{\frac{\alpha_1}{\alpha_2}}z - \alpha_1 r})$. Now $x_n \in (0, \sqrt{\sqrt{\frac{\alpha_1}{\alpha_2}}z - \alpha_1 r})$ for any $n \geq 1$ and we have proved that x_n will converge to the fixed point $\sqrt{\sqrt{\frac{\alpha_1}{\alpha_2}}z - \alpha_1 r}$.

Case (iii): $z^2 > 4\alpha_1\alpha_2 r^2$

In this case, it is not difficult to check that the function F has two fixed points, 0 and $\sqrt{\sqrt{\frac{\alpha_1}{\alpha_2}}z - \alpha_1 r}$. We will show that the iteration $x_{n+1} = F(x_n)$ converges to the fixed point $\sqrt{\sqrt{\frac{\alpha_1}{\alpha_2}}z - \alpha_1 r}$ for any initial $x_0 > 0$. The only time that the iteration converges to 0 is when $x_0 = 0$. As in Case (ii), F is not a contractive mapping on $[0, \infty)$. Again, let us have some observation and understand about the function F. A typical function F for this case is presented in figure 14.

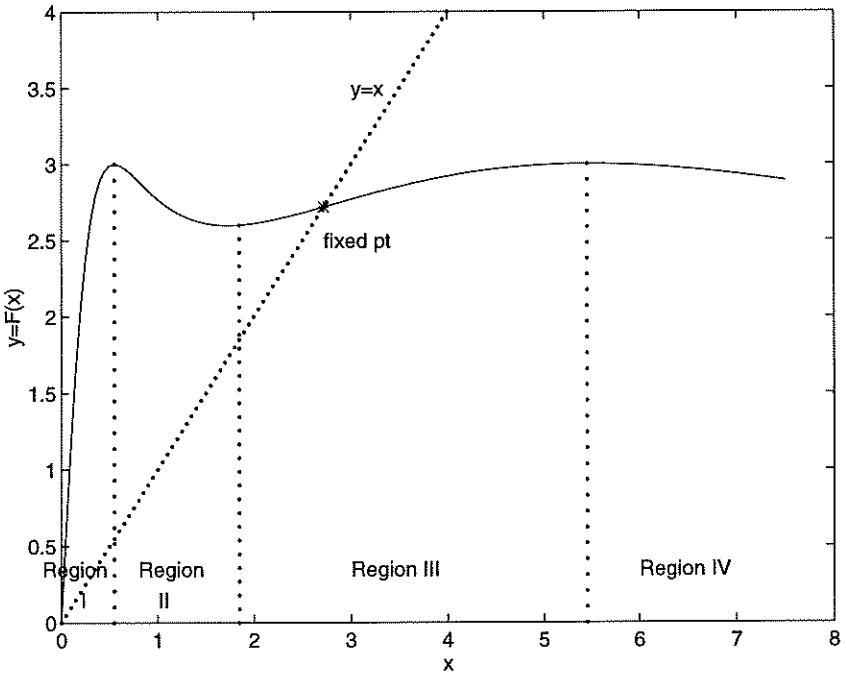

FIG. 14. *Typical F(x) when* $z^2 > 4\alpha_1\alpha_2 r^2$

(a) F has two maxima which attain at $x = \frac{z - \sqrt{z^2 - 4\alpha_1\alpha_2 r^2}}{2\sqrt{\alpha_2 r}}$, $\frac{z + \sqrt{z^2 - 4\alpha_1\alpha_2 r^2}}{2\sqrt{\alpha_2 r}}$ and F has one minimum which attains at $x = \sqrt{\alpha_1 r}$.

(b) It is not difficult to check that the order of the stationary points and the

fixed point is as follows:

$$\frac{z-\sqrt{z^2-4\alpha_1\alpha_2 r^2}}{2\sqrt{\alpha_2 r}} < \sqrt{\alpha_1 r} < \sqrt{\sqrt{\frac{\alpha_1}{\alpha_2}}z-\alpha_1 r} < \frac{z+\sqrt{z^2-4\alpha_1\alpha_2 r^2}}{2\sqrt{\alpha_2 r}}.$$

(c) We will divide the positive real axis into four regions:

Region I: $(0, \frac{z-\sqrt{z^2-4\alpha_1\alpha_2 r^2}}{2\sqrt{\alpha_2 r}})$

Region II: $(\frac{z-\sqrt{z^2-4\alpha_1\alpha_2 r^2}}{2\sqrt{\alpha_2 r}}, \sqrt{\alpha_1 r})$

Region III: $(\sqrt{\alpha_1 r}, \frac{z+\sqrt{z^2-4\alpha_1\alpha_2 r^2}}{2\sqrt{\alpha_2 r}})$

Region IV: $(\frac{z+\sqrt{z^2-4\alpha_1\alpha_2 r^2}}{2\sqrt{\alpha_2 r}}, \infty)$

(d) In Region III, F maps Region III into Region III and F is contractive. Therefore, if the initial guess x_0 lies inside this interval, then by fixed point theorem, the iteration will converge to the fixed point $\sqrt{\sqrt{\frac{\alpha_1}{\alpha_2}}z-\alpha_1 r}$.

(e) If x_0 lies in Region II, it can be checked that $x_1 = F(x_0)$ is in Region III and therefore the iteration will converge by (d)

(f) For any x in Region 1, $F(x)$ is either in Region I, II or III. Since $F(x) > x$ and is increasing on Region I, sooner or later, x_n will be in Region II or III. From that onwards, x_n will converge by (d) and (e).

(g) If x_0 is in Region IV, it can be shown that $x_1 = F(x_0)$ will be in Region I, II, or III. Therefore, by (d), (e) and (f), the iteration will converge.

□

By combining these two lemmas, Theorem 3.1 follows immediately.

REFERENCES

[1] P. Blomgren and T. Chan, *Modular Solvers for Constrained Image Restoration Problems*, UCLA CAM Report 97-52, November 1997.

[2] T. Chan and J. Olkin, *Circulant Preconditioners for Toeplitz-block Matrices*, Numer. Algorithms, Vol 6 pp. 89–101, 1994.

[3] T. Chan and C. Wong, *Total Variation Blind Deconvolution*, IEEE Transactions on Image Processing, Vol 7, pp. 370–375, March 1998.

[4] D. Fish, A. Brinicombe and E. Pike, *Blind deconvolution by means of the Richardson-Lucy algorithm*, J. Opt. Soc. Am. A Vol. 12, No.1 January 1996.

[5] D. Kundur and D. Hatzinakos, *Blind Image Deconvolutin*, IEEE Signal Processing Magazine, pp.43–64, May 1996. (See also, *Blind Image Deconvolution Revisited*, IEEE Signal Processing Magazine, pp. 61–63, November 1996).

[6] R. L. Lagendijk and J. Biemond, Iterative Identification and Restoration of Images, *Kluwer Academic Publishers*, 1991.

[7] R.L. Lagendijk, J. Biemond and D. E. Boekee, *Identification and restoration of noisy blurred images using the expectation-maximization algorithm*, IEEE Trans. Acoust. Speech Sig. Proc. Vol 38, 7 pp. 1180–1191, 1990.

[8] L. Rudin, S. Osher, *Total Variation Based Image Restoration with Free Local Constraints*, IEEE International Conference on Image Processing, Austin, TX, pp. 31–35, 1994.

[9] L. Rudin, S. Osher and E. Fatemi, *Nonlinear Total Variation Based Noise Removal Algorithms*, Physica D., 60, pp. 259–268, 1992.

[10] M. Ng, R. Plemmons and S. Qiao, *Regularization of RIF Blind Image Deconvolution*, IEEE Transactions on Image Processing, to appear.

[11] Y. You and M. Kaveh, *A regularization approach to joint blur identification and image restoration*, IEEE Transactions on Image Processing, Vol 5 pp. 416–428, March 1996.

[12] Y. You and M. Kaveh, *Blind Image Restoration by Anisotropic Regularization*, IEEE Transactions on Image Processing, Vol 8 pp. 396–407, March 1999.